Research Article

Advances in Nanoscience and Nanotechnology

Carbon and Core Shell like Molecular Nanostructures in Cancer diagnosis and Therapy

Badis Bendjemil[1, 2], Franck Cleymand[3], Thomas Pichler[5], Martin Knupfer[4] and Jörg Fink[4]

[1]*DGM/FST/UG-Université 08 Mai 1945 Guelma, 24000 Guelma, Algeria*

[2]*LASEA/DC/FS/UBMA-Annaba, 23000 Annaba, Algeria*

[3]*Department of Nanomaterials, Electronique et Vivant, Equipe, DOLPHIN-Nano-biomaterials for live-University of Lorraine, Institut Jean Lamour, UMR 7198 CNRS –University of Lorraine, 54011 Nancy Cedex, France*

[4]*Leibniz-Institute für Festkörper- und Werkstoffforschung (IFW-Dresden), Helmholtzstr. 20, 01069 Dresden, Germany*

[5]*Universität auf Vienna, Fakültät für Physik, Vienna, Austria*

***Corresponding author**

Prof. Badis Bendjemil, DGM/FST/UG-Université 08 Mai 1945 Guelma, 24000 Guelma, Algeria; Tel: +213674301959, E-mail: FPLO@Outlook.fr

Submitted: 13 Sep 2018; **Accepted**: 25 Sep 2018; **Published**: 05 Nov 2018

Abstract

During the past years, carbon nanotubes (CNTs) have attracted considerable interest since their first discovery. Great progress has been made in the field of nanomaterials given their great potential in biomedical applications. Carbon nanotubes (CNTs), due to their unique physicochemical properties, have become a popular tool in cancer diagnosis and therapy. They are considered one of the most promising nanomaterials with the capability of both detecting the cancerous cells and delivering drugs or small therapeutic molecules to these cells because of the unique structure, extremely high specific surface area to-volume ratio enable them to use in an intense real time applications such as detection and treatment of cancerous cells, nervous disorders, tissue repair. and excellent electrical and mechanical properties carbon nanotubes composed of excellent mechanical strength, electrical and thermal conductivities makes them a suitable substance toward developing medical devices., CNTs have been explored in almost every single cancer treatment modality, including drug delivery with small nanomolecules, lymphatic targeted chemotherapy, thermal therapy, photodynamic therapy, and gene therapy and demonstrate a great promise in their use in targeted drug delivery systems, diagnostic techniques and in bio-analytical applications. Majority of the biomedical applications of CNTs must be used after successful functionalization for more potential applications than pristine CNTs. There are several approaches to modify pristine CNTs to potentially active. CNTs poised into the human life and exploited in medical context. Here in, we reviewed the following topics (i) Functionalization of CNTs (ii) CNTs in real time applications such as drug delivery, gene therapy, biosensors and bio imaging; (iii) CNTs 3D printed scaffolds for medicine and (iv) Biocompatability and Biodegradability.

Single-walled carbon nanotubes (SWCNTs) were synthesized using the high-pressure carbon monoxide disproportionation process (HiPCO). The SWCNT diameter, diameter distribution and yield can be varied depending on the process parameters. The obtained HiPCO product present an iron nanoparticle encapsulated heteronanocarbon (core-shell nanoparticles) at low pressure (1 bar) after removing of iron metal catalyst nanoparticle and amorphous carbon by acid immersion and oxidation. The resulting therapeutic molecule in the form of core-shell nanoparticles and single walled carbon nanotubes after functionalization by filling of iron can be use as therapeutic nanomaterials in nanomedicine in diagnosis and treatment of cancer tumor. This paper describes the synthesis method and role of multifunctional nanoparticle in diagnosis and treatment of cancer. Therefore, the aim of this review is to provide basic information on nanoparticles, describe previously developed methods to functionalize nanoparticles and discuss their potential applications in nanobiomedical and mention the therapeutic nanoparticle large scale production and commercialization challenges. In the final part of the review, emphasis is given on the pharmacokinetic aspects of carbon nanotubes including administration routes, absorption mechanisms, distribution and elimination of carbon nanotubes based systems. Lastly, a comprehensive account about the potential biomedical applications has been given followed by insights into the future carbon nanotubes from synthesis to in vivo biomedical applications.

Keywords: Carbon nanotubes; HiPCO process; Optical absorption spectroscopy (OAS); Raman scattering; Magnetic iron core-shell nanoparticles; Purification; Sterilization; Functionalization; Fe@ SWCNTs; Therapeutic nanoparticles; Cellular mechanisms; Nanomedicine application; Cancer tumor therapy and diagnosis; Nanomaterials; Nanobiotechnology; Nanotechnology; Cancer diagnosis; Cancer therapy; In vivo nanobiomedical applications.

Introduction

The unique quasi one-dimensional nature of single wall carbon nanotubes (SWCNTs) has stimulated immense interest in these structures [1,4]. In addition, SWCNTs can themselves serve as templates for the formation of other nanostructures, further highlighting their versatility [5-7,80-82].

Their properties open their use in many applications from nanotechnologies to the biomolecular science as a result of their unique and exceptional physical, electronic and mechanical properties [2-4,8-10]. Their electronic properties depend sensitively on their diameter and chirality, giving rise to metallic and semi-conducting properties [11-13]. The semi conducting phases provide a superb opportunity for nanoscale device applications such as single molecule transistors and are considered ideal building blocks for nanomedicine application in diagnosis and therapy of cancer in the body.

The application of these nanoscale devices depends on a detailed knowledge of SWCNTs surface properties and the ability to functionalize them in a controlled manner. However, synthesizing SWCNTs in high yield with accurate diameter and chirality control remains a challenge.

Various important methods already exist for the primary SWCNTs growth like laser ablation, arc discharge and catalytic decomposition of hydrocarbons (CCVD) [14-20,25]. SWCNTs with high purity of about 90 wt. % have been formed in the gas phase using $Fe(CO)_5$ with high pressure of CO through the (HiPCO) process [21-23,76]. The synthesis of single-walled carbon nanotubes by CVD-HiPCO appears to be a promising method in comparison with arc-discharge and laser ablation. The low cost, high purity, relatively simple apparatus and multiple adjustable parameters are the main advantages for large-scale production.

The catalytic chemical vapor deposition characterized by the decomposition of a hydrocarbon on an MgO catalyst is similar to (HiPCO) supported on an iron, but it is unsuitable for large scale production, since the catalyst material is only available in limited amounts [24,25].

In contrast to this, the HiPCO process designed by Nikolaev et al. represents a continuousflow synthesis method [21]. It is possible modeling of the HiPco process for carbon Nanotube production at the reactor-scale analysis [79].

In the HiPCO process, a $Fe(CO)_5$ is injected into a stream of CO gas at high temperature (1170 to 1450 K) and pressure (1 to 40 bars). The iron forms metal clusters that act as catalytic sites to promote the Boudouard reaction (Fig.1a-b):

$$COc + CO_h \rightarrow C\ (solid) + CO_2\ (gas) \quad (1)$$
$$Fe(CO)_5 \rightarrow Fe + 5CO \quad (2)$$
$$2CO + Fe \rightarrow CNTs + CO_2 \quad (3)$$

where CO_c and CO_h is cold and hot carbon monoxide in the turbulent flow regime, respectively.

When the metal clusters achieve a size near that of C_{60}, SWCNTs nucleate and grown into the catalyst nonoparticles. The SWCNTs will continue to grow together with the metal clusters, which are growing with addition of residual free iron atoms. The average diameter of SWCNTs using HiPCO method is a function of CO pressure and is on average less than 1 nm, which is pure and smaller than SWCNTs synthesized by the laser vaporization process.

In the present paper we report the synthesis of single-walled nanotubes in a self-constructed HiPCO apparatus and discuss the structural composition and catalyst morphology, as well as the optical properties of deposited SWCNTs in relation to the synthesis parameters.

Multifunctional Nanoparticles

Multifunctional nanoparticle systems can integrate imaging, targeting and treatment modalities both on the surface and in the core to targeting tumor cells [32]. Multifunctional nanoparticles also use for simultaneous delivery of multiple treatment agents, to apply effective combinatorial therapeutic regimens against cancer [33]. Different factors contribute to multifunctional nanoparticle application resiliency, such as tumor location in the body, the inability of the treatment to reach the tumor cells, and the risk of damaging healthy cells (Fig. 1). Nanoparticles provide an opportunity to change the pharmacokinetic outline of drugs, reduce toxicity and enhance the therapeutic markers. This causes the development of "multifunctional" nanoparticles. For this reason, more capabilities like targeting and image contrast improvement are attached to the nanoparticles. On the other hand, additional functionality means additional synthetic steps and costs, more in vivo complex behavior and effects, and also greater regulatory impediments [34].

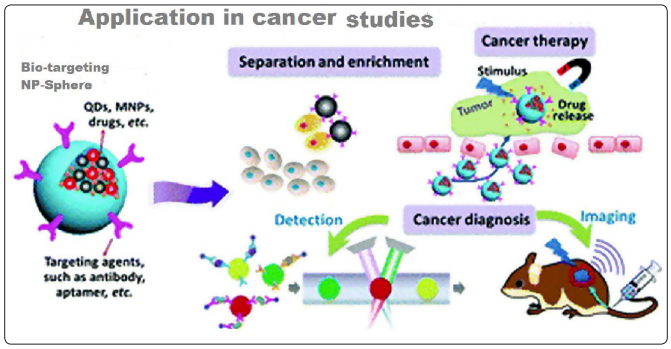

Figure 1: Nanoparticle application in cancer diagnosis and therapy

Cancer Therapy and Diagnosis

Some physicochemical features of available potentially potent therapeutic agents (both biopharmaceutical and small molecule drug related) such as large size, highly charged, too unstable metabolism and high insolubility, necessitate assistance of delivery vehicles to reach cancer target cells [36] (Table 1).

Table 1: Liposomes, Polymeric nanoparticles and dendrimers for combination cancer therapy

Formulation	Drugs	Indication	Type	Ref.
Core-shell nanoparticles	Paclitaxel and Bcl-2-targeted	siRNA Breast cancer	Polymeric nanoparticle	[45]
Nanoparticle aptamer types bioconjugates	Doxorubicin and docetaxel	Prostate cancer and various cancer types	Polymeric nanoparticle	[46]

As compared with conventional infusion method, the infusion of antineoplastic drugs with nanomaterials as carriers led to an increased payload of drugs to the tumor. In addition, by the Drug-loaded nanoparticles, surface molecules can be over expressed in tumor cells and therefore, by adding a targeting component, nanoparticles increased their efficacy of tumor specific drug delivery beyond EPR-mediated tumor homing, for example the polymeric particles such as BIND-014, with a PSMA-targeting moiety on the surface and a docetaxel payload, has been tested in humans clinical trials in early phase for metastatic cancers [37,38] (Table 2).

Table 2: Nanoparticles applications in drug delivery and cancer therapy

Drug delivery				
Agent delivered key	**Material[s]**	**Translational status**	**Details of study**	**Ref.**
Cisplatin	Carbon	Preclinical	Drug-loaded carbon nanohorns enhanced efficacy in human lung cancer mouse xenograft tumors in vivo compared to unmodified cisplatin	[59]
Paclitaxel	Carbon	Preclinical	Drug-loaded single-walled carbon nanotubes enhanced circulation halflife, tumor killing, and overall survival in 4T1 murine breast cancer model compared to unmodified paclitaxel	[60]
Doxorubicin	Carbon	Preclinical	Drug-loaded NDs enhanced blood circulation, tumor killing, and animal survival in chemoresistant mouse breast and liver tumors compared to unmodified doxorubicin	[61]
Epirubicin	Carbon	Preclinical	EGFR-targeted, drug-loaded ND-lipid hybrid particle enhanced tumor homing and tumor regression in a mouse model of human TNBC compared to free drug	[62]
Melittin peptide	Carbon	Preclinical	Drug-loaded perfluorocarbon nanoparticles improved circulation and therapeutic efficacy against human breast cancer mouse xenograft tumors and syngeneic graft mouse melanoma tumors compared to free drug	[64]
Bcl2L12	Gold	Preclinical	Gold-based spherical nucleic acid [SNA] delivery crossed BBB and accumulated in human glioma tumors in mice to silence target gene and reduce tumor burden	[65]
Proprietary siRNA	Carbon	Preclinical	Multiwalled carbon nanotubes loaded with siRNA inhibited tumor growth and prolonged overall survival in human lung cancer xenografted mice compared to siRNA alone or liposomaldelivery of siRNA	[63]

Carbon nanomaterials, including nanotubes, nanohorns, fullerenols, graphene, and NDs, have been used in delivering a wide spectrum of therapeutic compounds with regards to their versatile surface properties [39-44].

RNA interferences [RNAi] also can enhance drug delivery by silencing cancer-causing genes, if can overcome enzymatic degradation in the body (Table 3). Cyclodextrin-based polymers [CDPs] is a good example that are designed to protect and deliver siRNA tometastatic solid malignancies cancer cells [47-49]. Lipid based carriers with tumor-targeting and tumorpenetrating moieties have been designed to improve delivery and enhance the circulatory halflife of siRNA, for example siRNA nanocomplexes that display a cyclic nanopeptide on its surface is able to penetrate cells after being proteolytically processed by endogenous proteases [50].

Table 3: Cancer therapy Type of therapy Material s Translational status Key details of study Ref.

Cancer Theraphy Type of Therapy	**Material [s]**	**Translational Status**	**Key details of study**	**Ref.**
Immunotherapy, vaccine	Protein	Phase 2, clinical trial	Viral-like protein shell delivery of CpG-rich oligodeoxynucleotide [CpG-ODN] and melanocyte differentiation antigen resulted in enhanced CD8+T cell response in melanoma patients compared to antigen alone [NCT00651703]	[66]
Photothermal vascular	Silica, gold	Phase 1, clinical trials	Endothelial growth factor [VEGF]- targeted nanoshell's for thermal ablation and vessel disruption in mouse glioma model Currently in clinical trials for head and neck cancer[NCT00848042] and primary and/ or metastatic lung tumors [NCT01679470]	[67]
Radiotherapy	Hafnium oxide crystals	Phase 1, clinical trials	Nanoparticles for radio-induced tumor cell killing in mesenchymal and epithelial tumor xenograft mouse models Phase 1 clinical trials are ongoing as of 2011 [NCT01946867, NCT01433068]	[68]
Immunothera py, Vaccine	Polysacchar ide	Phase 1 clinical trial	Her2 antigen cholesteryl mannan and cholesteryl pullulan nanoparticle vaccines previously tested in Her2- expressing murine sarcomas Currently being evaluated in patients with advanced cancer with Her2-expressing tumor	[69, 70,71]
Magnetoresponsive	Iron/cobalt, PLGA	Phase 1 clinical trial	Magnetically guided polymer carriers loaded with Fe\\Co nanoparticle and doxorubicin for drug-nanoparticle deposition in right or left liver lobe of rabbits.	[73]
Immunothera py, RNA adjuvant	PEG-PLGA	Preclinical	Ovalbumin-loaded PEG-PLGA nanoparticles displaying RGD peptide for targeted M cell uptake and vaccination in mice.	[74]

Immunothera py, RNA adjuvant	Lipid	Preclinical	Ovalbumin-loaded PEG-PLGA nanoparticles displaying RGD peptide for targeted M cell uptake and vaccination in mice.	[75]
Immunothera py, Vaccine	PLG	Phase 1 clinical trial	PLG matrices that co-deliver granulocyte-macrophage colonystimulating factor [GM-CSF], CpGODN, and tumor lysate antigen for recruitment of DCs to PLG matrices, potent local and systemic antitumor CD8+ T cell response in mouse melanoma model. Starting phase 1 study of implantable vaccine to treat melanoma [NCT01753089]	[72]

Experimental

For the synthesis of SWCNTs, CO is used as carbon source and Fe $(CO)_5$ as the ironcontaining catalyst precursor. The formation of carbon is described by the equilibrium (equation 3), which is dependent on reaction temperature as well as the pressure. The equilibrium shifted to higher yields of carbon for temperatures less than 980 K, whereas above 980 K the CO decomposition is decreased. In addition the yield of carbon is increased by raising the CO pressure (principle of Le Chatelier).

The reaction rate is generally extremely low, but a suitable catalyst can affect it. This will be used favorably at the HiPCO-process. The way of formation of catalyst particles in the gas phase has a dominating influence on their size, yield, diameter and diameter distribution of SWCNTs and finally on the purity of the produced nanotubes. Therefore the injection of catalyst precursor into the hot reaction zone was systematically investigated besides the influence of reaction temperature and pressure. Figure 1a shows the reactor that consists of a quartz tube with an inside diameter of 32 mm and a length of 480 mm, which is heated on a tube length of 300 mm by a Kanthal resistance heater. Over the heater a steel tube is arranged for the preheating of CO, this is called the hot CO line (CO_h).

The facility allows working at pressures from 1 to 40 bars as high and temperatures up to 1450 K.

No SWCNTs were formed with increasing the transport rate by about a factor of five, whereas corresponding with results of Bronikowski et al. a reduction of the transport rate only decreases the yield of the deposited SWCNTs. The mixture of Fe $(CO)_5$ and CO is injected by means of an interchangeable copper nozzle through a ceramic insulated water cooled steel tube into the hot reaction zone [23]. The gas cooling is necessary to avoid the decomposition of Fe $(CO)_5$ at temperatures above 323 K. The CO_c nozzle is positioned 9 cm inside the heated reaction zone.

The injection velocity into the hot reaction zone and therefore the spontaneous heating of the cooled CO/Fe$(CO)_5$ mixture essentially influences the formation of SWCNTs. Different nozzle geometries can result in considerable changes of the gas flow rate and the temperature gradient between the CO/Fe$(CO)_5$ cooled gas and the reaction zone. Rapid heating and a broad injection jet enhanced the formation of SWCNTs. Therefore the influence of the nozzle geometry and the gas flow rate of COc on the yield; purity, diameter and diameter distribution of SWCNTs were investigated. Nozzles were tested with different hole diameters (from 0.4 to 1mm) and different number of holes (up to 5 holes) and for a constant hole diameter of 0.8mm but variable slot as shown in Figure 1b.

Around the COc nozzle a shield with holes is arranged for the injection of the preheated CO_h into the reaction zone. By aid of the nozzle system an intensive mixing of the gas flows was achieved. The COh gas flow rate varied between 100 and 500 sccm. The produced material consists of a black felt.

The aim of our investigations was the production of SWCNTs with high purity; reduced diameter distribution and with different mean diameter. It is possible to estimate diameter and diameter distribution as well as the size of the nanotubes bundles and to study theirs electronics character [27,28].

Results and Discussion

The growth of nanotubes was analyzed for samples obtained under different reaction pressure,temperature and CO gas flow rate. In addition, the study of the effect of the nozzle geometry (hole diameter, number of holes and slot width) and its role on the injection velocity was examined (Fig. 1).

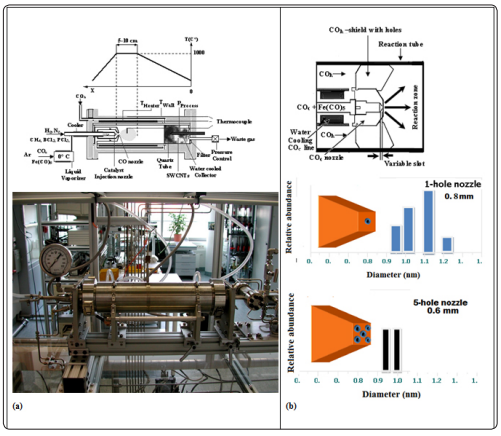

Figure 1: HiPCO reactor with different injection nozzle geometry used in our studies.(a) Schematic drawing of the HiPCO reactor with the temperature profile (b) Principle of the gas injection

Yield of Swcnt in Dependence on Pressure and Temperature

Fig. 2 shows the dependence of the total yield of the produced material and the yield of SWCNTs on the reaction pressure at two different reaction temperatures profile (T_r) in the reactor (Fig.1a).

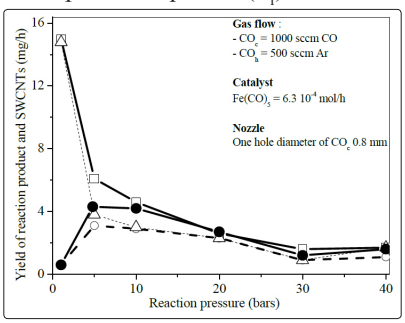

Figure 2: Total yield of deposited material in dependence on the reaction pressure (solid line square, doted line triangle) and of SWCNTs (circle and open circle) at reaction temperature 1173 K and 1323

At low pressures the reaction product mainly consists of graphite-like carbon. The SWCNT are dominating with increasing reaction pressure. Fig.3a and 3b show HRTEM images of two samples produced at the real temperature 1320 K at injection nozzle with pressure of 1 bar (The resulting therapeutic molecule in the form of core-shell nanoparticles with iron nanoparticle of diameter 20 nm embabed in graphite thickness of 4 nm; and bundles of single walled carbon nanotubes of 14 nm, after functionalization by iron encapsulation (filling) can be use as therapeutic nanomaterials in nanomedicine in diagnosis and treatment of cancer tumor); at 10 bars, respectively. Carbon nanotubes (CNTs) provide a smart carrier system on the nanometer scale. The system can be used as a template for ferromagnetic fillers. Such a molecular hybrid is a promising potential candidate for the controlled heating of tumour tissue at the cellular level. This is a key reason why it is important to optimize the synthesis route of metal filled carbon nanotubes with regards bulk scale synthesis and purity. In the current study we present multiwalled carbon nanotubes filled with α-iron phase (Fe-MWCNT) [78].

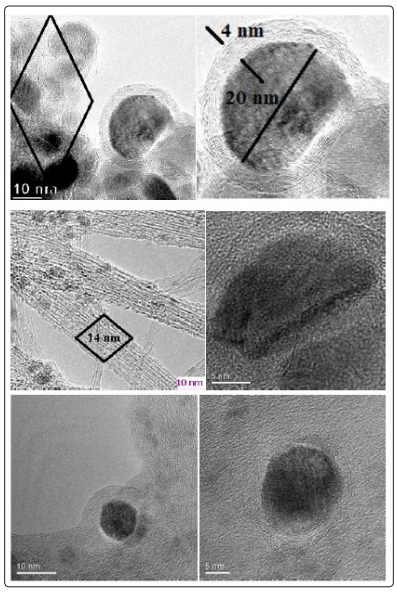

Figure 3: HRTEM micrograph: (a) – Carbon coated iron nanoparticles at pressure of 1 bar with max. (20 nm) in graphite with thickness of 4 nm , (b) - SWCNTs-bundles and iron nanoparticles at 10 bars.

A highly efficient and simple methodology based on wet chemistry to fill single-wall carbon nanotubes (Fe@SWCNTs) with iron, and thus create quantum wires in a bulk [7]. The research shown is unique in that it is the first experimental single-wall carbon nanotubes that have iron continuously within their core for extended length scale. While in sample Fig.3a, large Fe magnetic nanoparticles encapsulated in graphite are seen forming core shell like nanostructure; the bundles of SWCNTs formed at 10 bars are shown in Fig.3b. The observed decrease of the yield (Fig. 2) with the increase of reaction pressure is inconsistent with the principle of Le Chatelier. This is not surprising, because the deposition is a strongly kinetically controlled process by the measurement of CO_2 concentration to estimate the amounts of SWCNTs.

On the other hand the rise of the deposition rate of carbon with increasing temperature is in agreement with a thermodynamic equilibrium process.

Yield in Dependence on the Coc Gas Flow Rate

Different deposition rates are also observed at variation of the cold CO gas flow in the turbulent flow regime. An increasing flow leads to an enhancement of the formation of SWCNTs. Almost no SWCNTs were deposited at gas flows less than 500 sccm CO_c. By using this low gas flow rate, the catalyst decomposed in front of the reaction zone and formed large iron particles. The formation of SWCNT starts at flow rates above 500 sccm and the yield increases as shown in Fig. 4. The higher the CO_c gas flow rates the higher the SWCNTs quantity. The reaction product consists mainly of SWCNTs from COc gas flows up to 1500 sccm. The yield of SWCNTs decreases again at very high gas flows due to the reduced stay in the reaction zone.

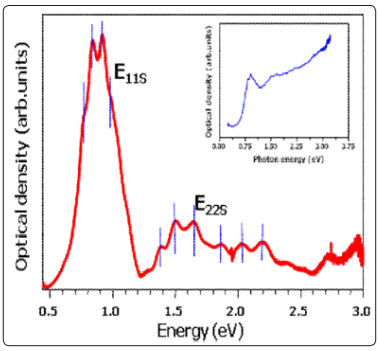

Figure 4: OAS signatue of SWCNTs for estimation of their mean diameter and diameter distribution meanly by pic fitting first semiconducting pics E_{11s}, E_{22s} ($\mathbf{I^S_{11}}$, $\mathbf{I^S_{22}}$). The metallic pic E_{22}m (I^m_{22}) is not used.

Diameter and Diameter Distribution Function of the Pressure

OAS is a good and express method to determine the diameter and diameter distribution of the SWCNTs. A detailed analysis of the optical absorption spectra is performed using the fitting of the tight binding model in comparison with the results of the Raman spectroscopy measurement. Optical absorption spectroscopy (OAS) of SWCNTs is a efficiency method to determines the diameter and diameter distribution of the as prepared SWCNTs **(Fig.4). Fig.5** shows the optical absorption spectra after subtracting the background as described **(Fig.4)**. previously [26,28]. The OAS intensity of the first two peaks ($\mathbf{I^S_{11}}$, $\mathbf{I^S_{22}}$) is related to the transitions between DOS van Hove singularities (**vHs**) in semiconducting nanotubes and the third (IM 11) one in the metallic nanotubes. The intensity of the (IS 22) peak describes the relative yield of the individual SWCNT as compared to amorphous carbon species [26]. The fine structure of the ($\mathbf{I^S_{22}}$) peak determines the diameter and diameter distribution.

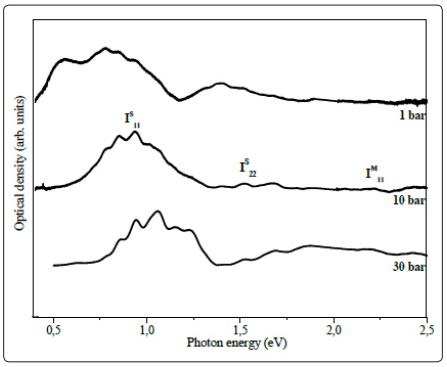

Figure 5: Optical absorption spectra, (reaction temperature: 1175 K, COc: 2000 sccm, CO_h: 500 sccm Ar, one hole nozzle diameter 0.8 mm).

In the laser ablation process the amount of catalyst particles is between 0 and 2 wt. % and the dielectric screening is independent from the process parameters.

In addition, from the peak position of corresponding second vHs (IS 22) one can calculate the diameters of the semi-conducting SWCNT according to the following equation [26,29].

$$(IS\ 22) = 4a0\ \gamma0/d \qquad (4)$$

With $\gamma0$ = 3 eV (overlap integral) and $\mathbf{a}_0$ = 0.142 nm (nearest-neighbor C-C distance).

As can be seen in the Fig.5 for the HiPCO process the spectra show a shift of the peaks positions to higher photon energies. This means a shift to smaller diameters with increasing reaction pressure as shown in Fig.5. The diameter distribution is relatively broad. Irrespective to the optimized preparation conditions the diameter distribution was found to shift downwards with increasing pressure.

The distribution is broader at higher pressure but the mean diameter of SWCNTs decreases with pressure (Fig. 6), which is in agreement with Nikolaev et al. [21].

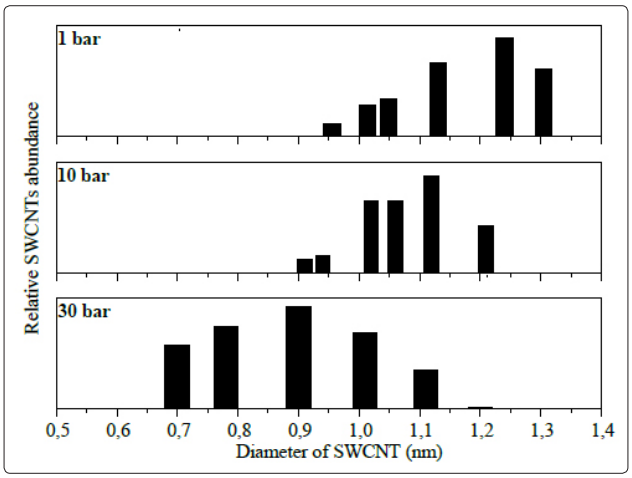

Figure 6: Diameter distribution and Mean diameter (d_{mean}) of SWCNTs versus reaction pressure calculated from the optical absorbance spectra (reaction condition see Fig. 5).

Iron-Content in the Deposited Material

Fig. 7 shows the energy dispersive spectroscopy of the deposit raw nanomaterials in dependence on the Fe content. The iron content was determined by AAS after removing of the carbon by oxidation. Since the OAS measurements were always performed with the same thickness films on the KBr or NaCl single crystal and the same preparation procedure, the intensities of the ($\mathbf{I}^S_{22}$) transition or ($\mathbf{I}^S_{11}$) can be directly compared and calculated. In the HiPCO process the amount of amorphous carbon species is low and the main contribution of the intensity variation of the ($\mathbf{I}^S_{22}$) peak is due to different dielectric screening of the Fe catalyst nanoparticles. When the amounts of iron contents are lower the intensity becomes higher. The OAS can be used to determine the iron content in the different SWCNTs containing materials considering certain conditions. The spectra in Fig.8 can be used as additional information about the raw nanomaterial by electron energy loss spectroscopy curves for the determination of the Fe concentration.

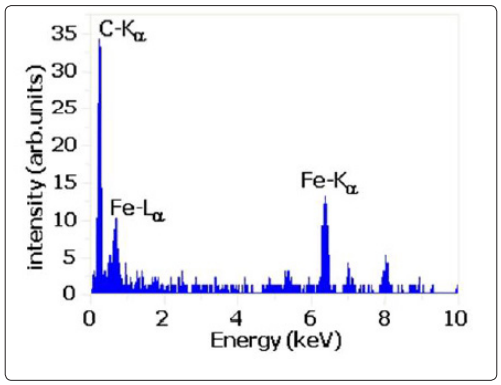

Figure 7: EDX spectra of the as grown HiPCO heronanocarbon

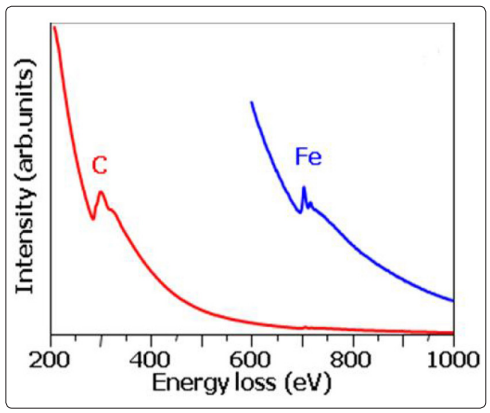

Figure 8: EELS spectra of the as grown HiPCO heronanocarbon

Effect of Nozzle Injection Geometries

The geometries of injection nozzle used can affect the injection velocity and thereafter the yield of SWCNTs by varying the dimension of the catalyst nanoparticles and the volume of the CO in the reaction zone.

The different types of nozzles were tested to optimize the injection of the COc into the reaction zone. An optimized injection stream should increase the SWCNTs yield and reduce the nanotube diameters. If the injection is defocused small catalyst particles are formed, whereas a focused stream promotes the formation of large iron nanoparticles. The changing of the injection into the hot reaction zone is performed by variation of the slot width (Fig.1b), on the other hand by using of nozzles with different holes diameters and number of holes. Table 4 contains the observed yields of as grown SWCNTs raw material and the highest intensities $\mathbf{I}^S_{22}$, which correspond to the Fe content in comparison to the mean diameters for different slots. The best results are achieved at a slot width equal to 21 μm, both the purity (lowest Fe content) and yield have a maximum value. The yield of the SWCNTs is estimated by the maximum intensity of the diameter distribution of the second transition peak (IS 22). The purity I (IS 22) of 0.068 and 0.056 (arb. units), yield of 8.3 and 4.8 (mg/h) and mean diameter of 1.13 and 1.02 (nm) are calculated at pressure 5 and 10 bars, respectively.

Table 4: Observed yields of as grown SWCNTs raw material and the highest intensities I^S22, which correspond to the Fe content in comparison to the mean diameters for different slots

P (bars)	Slot width (µm)	I_{max} (I^S 22) (*a.u.*)	d_{mean} (nm)	Yield (mg/h)
10	7	0.015	1.01	3.3
	14	0.029	1.01	2.7
	21	0.056	1.02	4.8
	42	0.006	1.14	1.7
5	**21**	**0.068**	**1.12**	**8.3**
	42	0.004	1.12	2.8

Table 5 shows a comparison between one and five holes nozzle with a hole diameter 0.6 mm. The number of holes seems to have a large influence on the diameter and the diameter distribution of the SWCNTs. At the same deposition conditions the mean diameter is reduced from 1.13 to 0.92 nm if a nozzle with five holes is used. Also a smaller diameter distribution can be observed in comparison with one hole injection nozzle. The maximum yield has a value of about 3.4 (mg/h) and mean diameter 1.13 nm at reaction pressure 10 bars and one hole of diameter 0.6 mm. The optimized nozzle geometry versus SWCNTs yield is given at one hole diameter 0.8 mm and slot width equal to 21 mm.

Table 5: Comparison between one and five holes nozzle with a hole diameter 0.6 mm. The number of holes seems to have a large influence on the diameter and the diameter distribution of the SWCNTs

P (bars)	Holes number (ϕ=6 mm)	Imax (IS 22) (a.u.)	dmean (nm)	drange (nm)	Yield (mg/h)
10	1	0.021	1.12	0.4	3.4
	5	0.009	0.92	0.06	1.5

Tables 1 and 2 show that the nozzle geometry (hole diameter, number of holes and slot width) has a primordial effect on the injection velocity.

The Optimal Deposition Condition and Purification Procedure

Summarizing the results from above, one can derive the optimal conditions for the synthesis of SWCNTs by HiPCO process as follows:

-a reaction pressure of 1 or 10 bars;

-a reaction temperature of 1250 K;

-a COc flow rate of 2000-2500 sccm CO included $Fe(CO)_5$+500 sccm Ar and CO_h flow rate of 100 sccm, an one-hole nozzle diameter of 0.8 mm with 21 µm slot. Under these conditions the yield of SWCNTs amounted to about 10 mg/h.

In Fig. 5 typical optical absorption spectra of material grown under such conditions are shown with the same synthesis parameters. The Fe concentration of the product is less than 5 % and the mean diameter decreased from 1.12 to 1.02 nm with increasing pressure from 5 to 10 bars. With increasing pressure the diameter distribution also decreases (Fig.5).

In order to remove the iron catalyst and carbon-like impurities the purification of the raw material is realized in two steps:

Oxidation followed with acid treatment in HCl (36 %). The raw materials were purified by oxidation in high vacuum at 523 K in a wet Ar/20 vol. % O2 mixture to remove SWCNT carbon-like impurities and to oxidize the iron catalyst nanoparticles. At atmosphere pressure according to the oxidation time amounted to 6 hours [30,31]. Subsequently the remaining iron oxide nanoparticles were solved and removed by chemical treatment in concentrated HCl/ alcohol, C_2H_5OH mixture solution in ratio 1/1 by sonication for 2 h at 353 K.

Fig. 9 shows HRTEM imagines, EDX and EELS spectra of raw and purified SWCNTs. The purification effect is obvious. However in all purified samples few Fe nanoparticles can be still observed which are covered with a relatively thick carbon layer (core shell nanostructure). A complete removal of the catalyst leads to an undesirable burning of grown SWCNTs during the oxidation step. This degree of purification is also confirmed by the increasing of the optical absorbance intensity area of the first peak (I^S_{11}) and second peak (I^S_{22}) in the optical signature of the SWCNTs (Fig.10). The absorption peaks of the purified samples have higher intensity than the raw material (Fig.10) indicating the much higher purity of the purified sample. The mean diameter and diameter distribution do not change significantly by the oxidation treatment (see the inset in Fig.10). This observation confirms that the oxidation treatment has no detrimental effect on the nanotube crystallinity.

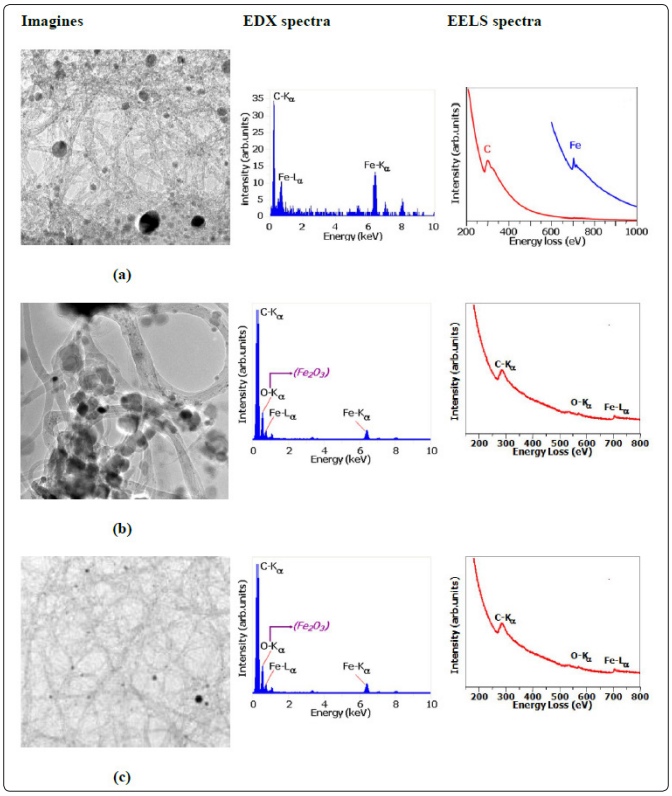

Figure 9: (a)- HRTEM imagines, EDX and EELS spectra of SWCNTs raw material, (b)- After purification. The optical absorption spectra of the purified sample have a higher intensity as the raw material (Fig.11) indicating the much higher purity of the purified sample. The mean diameter does not change significantly.

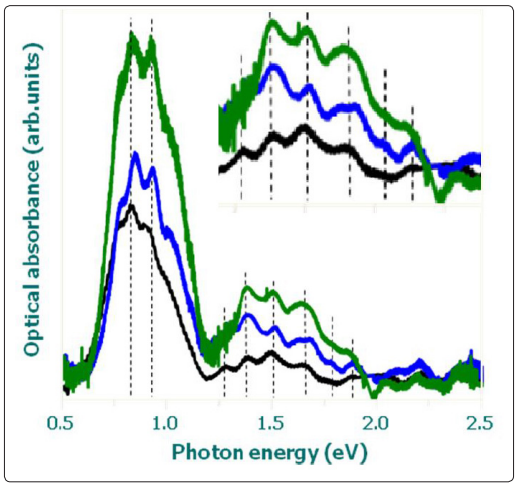

Figure 10: Optical absorption spectra of a purified sample (green line), oxidized SWCNTs (blue line) and optimized raw material (black line). In insert is represented the fine structure of the ($\mathbf{I^S}_{22}$) of the semiconducting pic $\mathbf{E^s}_{22}$.

Purification Procedure and Separation of the Core Shell Nanostructure

The soot-like products, obtained in HiPCO parameters processes, have to be subjected to purification of the product carbon nanotubes for functionalization, separation and sterilization of the therapeutic-molecule (core-shell iron magnetic nanoparticle encapsulated in graphite like heteronanocarbon) in order to remove amorphous carbon, non-encapsulated metal and carbide. The purification procedures have to remove, such as impurities. In order to remove amorphous carbon in the samples it is necessary to anneal the resulting reaction products for 6 hr in 50% nitric acid HNO_3 at 323K, and then to flush by distilled water until complete removal of the acid is achieved.

In order to remove noncoated iron or carbides, the samples have to be boiled in 2M HCl (24 h), and then washed in distilled water and subsequently in ethanol and annealed in dry air atmosphere at 350K. In order to also remove amorphous carbon, the chemical oxidation by KMnO4 dissolved in 50% sulfuric acid could be used [77]. Again the sample has to be washed thoroughly in distilled water and annealed in dry air atmosphere.

Characterization of carbon nanotubes and core shell like nanostructure molecule by Raman spectroscopy

The Raman spectra present different features being all sensitive to chiral indices (n,m) specifying the perimeter vector (chiral vector), such as the radial breathing mode (RBM) where all the carbon atoms are moving in-phase in the radial direction, the G-band where neighbouring atoms are moving in opposite directions along the surface of the nanotube as in 2D graphite, the dispersive disorder induced D-band and its second-order related harmonic G′-band. From these five features (**Fig.11a and b**), the RBM is the one which appears more sensitive to the nanotube diameter (d), according to the expression RBM

$$\omega RBM = A/d + B \quad (5)$$

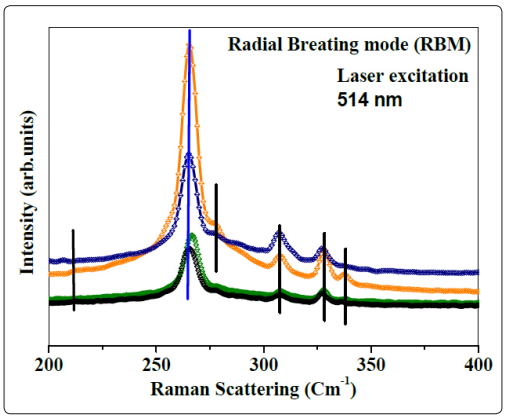

Figure 11a: RBM spectra (Laser excitation 514 nm). The regions indicate groups of metallic (200-250 cm^{-1}) and semiconducting (250-400 cm^{-1}) nanotubes with different diameter, diameter distribution and synthesis pressure.

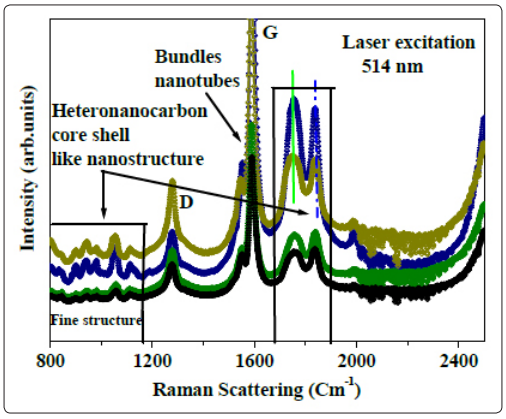

Figure 11b: D and G bands (laser excitation 514 nm). The fine structure in between (800-1200 cm^{-1}) and (1680-1800 cm^{-1}) regions indicate the vibration frequency of the core shell like structure heteronanocarbon groups.

Where ω is the vibration frequency, and A and B are constants and vary between individual nanotubes and bundle nanotubes. Some authors consider only the constant A in determination of the diameter [83-88].

Bat there's no formula for calculation of the diameter of nanocapsule (iron /graphit) or core Shell nanostructure in the literature.

Determination of Diameter and Diameter Distribution

Four characteristic features of a HiPCO/SWCNT sample may be found in Raman spectra presented in Fig. 11a. An analysis of RBM band is visible in the red laser spectra. (Laser excitation 514 nm) for typical HiPCO/SWCNT bundles of the diameter d = 1.13±0.4 nm, A = 224 cm^{-1} and B = 14 cm^{-1} have been calculated88, B is an up shift in ωRBM due to nanotube–nanotube interactions. The calculated diameter distribution was obtained using Eq. (5) (Table 6, Fig.11a). The range of diameters varies between 0.7 nm and 1.13 nm. According to the Kataura plot, we have only obtained signals from semiconducting and small signal of metallic nanotubes with the green laser with different chirality (n, m). We indicate in future the use of various lasers energies analysis is very important, because each experiment can give different data on optical and physical

properties. The ratio between D and G band and the RBM and its relation to the diameter distribution are very important factors allowing one to distinguish between carbon nanotubes and core shell nanostructured therapeutic molecule.

Table 6: Diameter distribution calculated from the RBM (Fig.11a) feature using Eq. (5)

Raman Shift (cm^{-1})	Diameter (nm)
337.352	0.7000
327.397	0.7225
307.421	0.7724
278.452	0.8484
264.225	0.9239
211.121	1.1370

It was found that the diameter and diameter distribution obtained by optical absorbance spectroscopy (Fig.5, 6 and Table 4, 5) are similar to that calculated after Raman scattering.

Commercialization challenges

Continuous advancements in nanomedicine have opened up opportunities for application of new generation of multifunctional therapeutic nanoparticles in a variety of medical disciplines, but still we are facing some basic challenges. There is a huge gap between nanobiotechnology researches in labs and the production of commercialized therapeutic nanoparticles. This gap contains a whole litany of challenges that must be tackled. One of the most important challenges lies in scaling up processes for production commercially. For a viable scale-up, laboratory processes must be consistent with current manufacturing capabilities.

Another challenge is navigating an often mystifying regulatory perspective. Although nanoparticle based therapies refer to more complicated requirements than conventional medical treatments in that both require clinical trials that demonstrate safety and efficacy, more complicated technology needs more evidence of effectiveness. The human, environment and animal safety that related to the life cycle issue also are the main point for discuss. Detect and determine the toxicity of engineered nanomaterials within next 5 to 15 years is an important challenge for researchers, though, describes models for predicting effects of nanomaterials on human health and the environment would be an inevitable issue. Finally, researchers should take a proactive role in translating laboratory discoveries into feasible medical technology.

Such an important role requires researchers to consider future commercialization early in their research and act accordingly.

The Future of Nanomedicine

In spite of a huge number of researches about nanomedicine, unmet medical demands in cancer diagnosis and therapy remain substantial.

The potential for nanotechnology in medicine, in the future of cancer diagnosis and therapy is unprecedented. Continuously drives advances in diagnostic nanobiotechnological devices design, with diameters of hundreds of atoms is a considerable progress that can revolutionized the ability of cancer diagnosis especially about medical data collection, detect chemical changes in the body, the ability of closer real-time tracking of a patient's status and the build of nanoscale microscopic cameras. All of these advancements can provide a complete map of most of the tissue in the human body, in a level of detail that's impossible with X-ray or MRI. With the application of quantum dots as an optical barcode may indeed gene sequencing and chemical analysis be speed up and finally it provides the possibility of faster, cheaper and more reliable diagnostic tests outside the body. The outcome of these progressions at cellular and molecular levels will be result in the potential for diagnosing and treating many conditions preemptively, before they have the opportunity to proliferate.

Summary

Our systematic study of the HiPCO process shows that several parameters strongly affect the properties of the deposited material (purity, yield and diameter) e. g. the reaction pressure, the temperature at injection nozzle and the injection velocity of the CO/Fe $(CO)_5$ gas mixture in the reaction zone. These parameters are important for nucleation and deactivation of the iron nanoparticles/SWCNT growth to be dealt with lightly.

With increasing of the CO through Fe $(CO)_5$ pressures the diameter of SWCNTs decreases. The new contribution in our work on the synthesis of SWCNTs by CVD (HiPCO method) is given by varying of the injection nozzle geometry to optimize the dimension of the iron catalys nanoparticles and the volume of the gas phase in the reaction zone where the SWCNTs nu leate. This has produced parameters nanotubes as small as 1.0 nm in diameter. The purity and yield of the deposited material are increased with increasing of CO_c gas flow by means of rapid heating of the gas mixture and using an optimum injection profile. The optimal conditions to produce highly pure SWCNTs were found at 1250 K pressures between 1, 10 bars and a gas flow in the cold line of 2000-2500 sccm CO and 500 sccm Ar. Higher gas in turbulent flows regime at adjusted injection nozzle geometry should represent a new interesting result for instance. We continue to synthesizing this therapeutic molecule at low pressure (1 bar) with variation of other parameters in order to obtain uniform and fine molecules according to the size of the cell of human tissues. The HiPCO process is one of the best-investigated procedures, for carbon nanotubes synthesis and functionalization of single walled carbon nanotubes after by filling of iron can be use as therapeutic nanomaterials in nanomedicine in diagnosis and treatment of cancer tumor. The resulting therapeutic molecule in the form of core-shell nanoparticles with iron nanoparticle of diameter 20 nm embabed in graphite thickness of 4 nm; and bundles of single walled carbon nanotubes of 14 nm, after functionalization by iron encapsulation (filling) can be use as therapeutic nanomaterials in nanomedicine in diagnosis and treatment of cancer tumor; at 1 and 10 bars, respectively.

The magnetic measurement and Raman scattering measurements will be performed in the near future according to their nanomedicine application by photothemal vascular cancer therapy (hyperthermia) and cellular dimension in the body after purification, separation and sterilization. By this process we have obtained at low pressure metal ferromagnetic in core shell structure by injection of nanocatalyst Metalcene, Me $(CO)_5$ (Me=**Fe**, Ni and Co).

This information is not only for the special equipment used but also can be generalized to large industrial-scale of the HiPCO process with high yield and uniformed therapeutic molecule diameter iron nanoparticle and heteronanocarbon thickness. There is a huge gap

between nanobiotechnology researches in labs and the production of commercialized therapeutic nanoparticles. This gap contains a whole litany of challenges that must be tackled. One of the most important challenges lies in scaling up processes for production commercially. For a viable scale-up, laboratory processes must be consistent with current manufacturing capabilities.

Finally, researchers should take a proactive role in translating laboratory discoveries into feasible medical nanotechnology. Such an important role requires researchers to consider future commercialization early in their research and act accordingly.

Acknowledgments

We acknowledge support of PHC-TASSILI PROJEKT (2019-2023) between the laboratory LASEA-University of Badji-Mokhtar of Annaba/University 8 Mai 1945 of Guelma-Algeria….and the laboratory DOLPHIN-NANO-BIO-MATERIALS FOR LIVE-University of Lorraine-Nancy-France in addition the IFW-Dresden-Germany and the Universität auf Vienna, Fakültät für Physik, Vienna, Austria.

The partner Pr. Abdelaziz LANKAR from the (Laboratoire Central de Cytologie Pathologiques CHU Annaba-Algeria) are also acknowledge for the help in the nanoparticles applications in cancer diagnosis and therapy.

References

1. Iijima S, Ichihashi T (1993) Single-shell carbon nanotubes of 1-nm diameter. Nature 363: 603-605.
2. Sinha N (2005) Carbon nanotubes for biomedical applications. IEEE Transactions on Nanobioscience 4: 180-195.
3. Saito S (1997) Carbon Nanotubes for Next-Generation Electronics Devices. Science 278: 77-78.
4. Saito R, Dresselhaus G, Dresselhaus MS (1998) Physical properties of carbon nanotubes. (London, Imperial College).
5. Borowiak-Palen E, Pichler T, Fuentes GG, Bendjemil B, Liu X et al., (2003) Infrared response of multiwalled boron nitride nanotubes Chem Commun. 1: 82-84.
6. Rümmeli MH, Borowiak-Palen E, Gemming T, Knupfer M, Biedermann K, et al., (2005) on the formation process of silicon carbide nanophases via hydrogenated thermally induced templated synthesis. Appl Phys 80: 1653-1656.
7. Borowiak-Palen E, Mendoza E, Bachmatiuk A, Rümmeli MH, Gemming T, et al., (2006) Iron filled single-wall carbon nanotubes - A novel ferromagnetic medium. Chem Phys Lett 421: 129-133.
8. Chico L,Crespi VH, Benedict LX, Louie SG, Cohen ML (1996) Pure Carbon Nanoscale Devices: Nanotube Heterojunctions. Phys Rev Lett 76: 971-974.
9. Wong EW, Sheehan PE, Lieber CM (1997) Nanobeam Mechanics: Elasticity, Strength, and Toughness of Nanorods and Nanotubes Science 277: 1971-1975.
10. Salvetat JP, Bonard JM, Thomson NH, Kulik AJ, Forró L et al. (1999) Mechanical properties of carbon nanotubes. Appl Phys 69: 255-260.
11. Mimitmire JW, Dunlop BI, White CT (1992) Are fullerene tubules metallic? Phys Rev Lett 68: 631-636.
12. Hamada N, Sawada SI, Oshiyama A (1992) New one-dimensional conductors: Graphitic microtubules. Phys Rev Lett 68: 1579-1589.
13. Dresselhaus MS, Dresselhaus G, Eklund PC (1996) Science of fullerenes and carbon
    a. nanotubes: their properties and applications, San Diego, Academic Press.
14. Thess A, Lee R, Nikolaev P, Dai H, Petit P et al. (1996) Crystalline Ropes of Metallic Carbon Nanotubes Science 483-487.
15. Rinzler AG, Liu J, Nikolaev P, Huffmann CB, Rodriguez-Macias FJ et al. (1998) Large-scale purification of single-wall carbon nanotubes: process, product, and characterization. Appl Phys 67: 29-37.
16. Guo T, Nikolaev P, Thess A, Colbert DT, Smalley RE (1995) Catalytic growth of singlewalled nanotubes by laser vaporization. Chem Phys Lett 243: 49-54.
17. Journet C, Masser WK, Bernier P, Loiseau A, Lamy de la chapelle M, et al. (1997) Large-scale production of single-walled carbon nanotubes by the electric-arc technique Nature 388: 756-758.
18. Iijima S (1991) helical microtubules of graphitic carbon. Nature 354: 56-58.
19. Hafner JH, Bronikowski MJ, Azamian BR, Nikolaev P, Rinzler AG et al. (1998) Catalytic growth of single-wall carbon nanotubes from metal particles. Chem Phys Lett 296: 195-202.
20. Colomer JF, Bister G, Willems I, Konya Z, Fonsera J, VanTendeloo G et al., (1999) Synthesis of single-wall carbon nanotubes by catalytic decomposition of hydrocarbons. Chem Comm 1343-1350.
21. Bronikowski MJ, Nikolaev P, Bradley RK, Rohmound F, Colbert DT et al. (1999) Gas-phase catalytic growth of single-walled carbon nanotubes from carbon monoxide. Chemical Physics Letters 91-97.
22. Cheng HM, Li F, Sun X, Brown SDM, Pimenta MA, Marucci A, et al. (1998) Bulk Morphology and diameter distribution of single-walled carbon nanotubes synthesized by catalytic decomposition of hydrocarbons. Chem Phys Lett 289: 602-610.
23. Bronikowski MJ, Willis PA, Colbert, K. A. Smith, Smalley RE (2001) Gas-phase production of carbon single-walled nanotubes from carbon monoxide via the HiPco process: A parametric study J Vac Sci Technol 19: 1800-1814.
24. Colomer JF, Stephan C, Lefrant S, Tendeloo GV, et al. (2000) Large-scale synthesis of singlewall carbon nanotubes by catalytic chemical vapor deposition (CCVD) method. Chem Phys Lett 317: 83-89.
25. Yan H, Li Q, Zhang J, Lin Z (2002)Possible tactics to improve the growth of single-walled carbon nanotubes by chemical vapor deposition Carbon 40: 2693-2698.
26. Jost O, Gorbunov AA, Pompe W, Pichler T, Friedlein R, et al. (1999) Diameter grouping in bulk samples of single-walled carbon nanotubes from optical absorption spectroscopy. Appl Phys Lett 75: 2217-2224.
27. Kuzmany H, Burger B, Hulman M, Kürti J, Rinzler AG et al. (1998) Spectroscopic analysis of different types of single-wall carbon nanotubes. Eur Phys Lett 44: 518-528.
28. Kuzmany H, Plank W, Hulman M, Kramberger Ch, Gruneis A, Pichler T, et al., (2001) Determination of SWCNT diameters from the Raman response of the radial breathing mode Eur Phys J 22: 307-320.
29. Liu X, Pichler T, Knupfer M, Golden MS, Fink J, et al. Detailed analysis of the mean diameter and diameter distribution of single-wall carbon nanotubes from their optical response. Phys Rev B 662002045411: 1-8.
30. Chiang IW, Brinson BE, Huang A, Willis PA, Bronikowski MJ,

Margrave JL et al. (2001) Purification and Characterization of Single-Wall Carbon Nanotubes (SWNTs) Obtained from the Gas-Phase Decomposition of CO (HiPco Process). J Phys Chem 105: 8297-8301.
31. Bendjemil B, Borowiak-Palen E, Graff A, Pichler T, Fink J et al., (2004)Elimination of metal catalyst and carbon-like impurities from single-wall carbon nanotube raw material. Appl Phys 78: 311-314.
32. Nie S, Xing Y, Kim GJ, Simons JW (2007) Nanotechnology applications in cancer. Annu. Rev Biomed Eng 9: 257-288.
33. Srinivasan M, Rajabi M, Mousa SA (2015) Multifunctional nanomaterials and their applications in drug delivery and cancer therapy. Nanomatherials 5: 1690-1703.
34. Yu MK, Park J, Jon S (2012) Targeting strategies formultifunctional nanoparticles in cancer imaging and therapy. Theranostics 2: 3-44.
35. Wen CY, Xie HY, Zhang ZL, Wu LL, Hu J (2016) Fluorescent/ magneticmicro/nano-spheres based on quantum dots and/or magnetic nanoparticles: preparation, properties, and their applications in cancer studies. Nanoscale 8: 12406-12429.
36. Nie S, Xing Y, Kim GJ, Simons JW (2007) Nanotechnology applications in cancer. Annu Rev Biomed Eng 9: 257-288.
37. Senzer N, Nemunaitis J, Nemunaitis D, Bedell C and Edelman G (2013) Phase I study of a systemically delivered p53 nanoparticle in advanced solid tumors Mol Ther 21: 1096-1103.
38. Hrkach J, Von Hoff D, Ali MM, Andrianova E, Auer J (2012) Preclinical development and clinical translation of a PSMA-targeted docetaxel nanoparticle with a differentiated pharmacological profile. Sci Transl Med 4: 128-139.
39. Chaudhuri P, Paraskar A, Soni S, Mashelkar RA, Sengupta S (2009) Fullerenol-cytotoxic conjugates for cancer chemotherapy. ACS Nano 3: 2505-2514.
40. Soman NR, Baldwin SL, Hu G, Marsh JN, Lanza GM (2009) Molecularly targeted nanocarriers deliver the cytolytic peptide melittin specifically to tumor cells in mice, reducing tumor growth. J Clin Invest 119: 2830-2842.
41. Ajima K, Murakami T, Mizoguchi Y, Tsuchida K, Ichihashi T (2008) Enhancement of in vivo anticancer effects of cisplatin by incorporation inside single-wall carbon nanohorns. ACS Nano 2: 2057-2064.
42. Liu Z, Chen K, Davis C, Sherlock S, Cao Q (2008) Drug delivery with carbon nanotubes for in vivo cancer treatment. Cancer Res 68: 6652-6660.
43. Chow EK, Zhang XQ, Chen M, Lam R, Robinson E (2011) Nanodiamond therapeutic delivery agents mediate enhanced chemoresistant tumor treatment. Sci Transl Med 3: 21-73.
44. Huang H, Pierstorff E, Osawa E, Ho D (2007) Active nanodiamond hydrogels for chemotherapeutic delivery. Nano Lett 7: 3305-3314.
45. Wang Y, Gao S, Ye WH, Yoon HS, Yang YY (2006) Co-delivery of drugs and DNA from cationic core-shell nanoparticles self-assembled from a biodegradable copolymer. Nat Mater 5: 791-796.
46. Zhang L, Radovic-Moreno AF, Alexis F, Gu FX, Basto PA (2007) Co-delivery of hydrophobic and hydrophilic drugs from nanoparticle-aptaer bioconjugates. Chem Med Chem 2: 1268-1271.
47. Davis ME, Zuckerman JE, Choi CH, Seligson D, Tolcher A (2010) Evidence of RNAi in humans from systemically administered siRNA via targeted nanoparticles. Nature 464: 1067-1070.
48. Heidel JD, Liu JY, Yen Y, Zhou B, Heale BS (2007) potent siRNA inhibitors of rib nucleotide reductase subunit RRM2 reduces cell proliferation in vitro and in vivo. Clin. Cancer Res 13: 2207-2215.
49. Koldehoff M, Steckel NK, Beelen DW, Elmaagacli AH (2007) Therapeutic application of small interfering RNA directed against bcr-abl transcripts to a patient with imatinib-resistant chronic myeloid leukaemia. Clin Exp Med 7: 47-55.
50. Ren Y, Cheung HW, von Maltzhan G, Agrawal A, Cowley GS et al, (2012) Targeted tumorpenetrating siRN nanocomplexes for credentialing the ovarian cancer oncogene ID4. Sci Transl Med 4: 147-158.
51. Senior J, Crawley JC, Gregoriadis G (1985) Tissue distribution of liposomes exhibiting long halflives in the circulation after intravenous injection. Biochim Biophys Acta 839: 1-8.
52. Gobin AM, Lee MH, Halas NJ, James WD, Drezek RA et al., (2007) Near-infrared resonant nanoshells for combined optical imaging and photothermal cancer therapy. Nano Lett. 7: 1929-1934.
53. Loo C, Lowery A, Halas N, West J, Drezek R (2005) Immunotargeted nanoshells for integrated cancer imaging and therapy. Nano Lett 5: 709-711.
54. Hu X, Gao X (2011) Multilayer coating of gold nanorods for combined stability and biocompatibility. Phys Chem 13: 10028-10035.
55. Kannadorai RK, Liu Q (2013) Optimization in interstitial plasmonic photothermal therapy for treatment planning. Med Phys 40: 103301.
56. Chen CL, Kuo LR, Lee SY, Hwu YK, Chou SW (2013) Photo thermal cancer therapy via femtosecond-laser-excited FePt nanoparticles. Biomaterials 34: 1128-1134.
57. Pouponneau P, Leroux JC, Soulez G, Gaboury L, Martel S (2011) Co-encapsulation of magnetic nanoparticles and doxorubicin into biodegradable microcarriers for deep tissue targeting by vascular MRI navigation. Biomaterials 32: 3481-3486.
58. Maggiorella L, Barouch G, Devaux C, Pottier A, Deutsch E (2012) Nanoscale radiotherapy with hafnium oxide nanoparticles. Future Oncol 8: 1167-1181.
59. Ajima K, Murakami T, Mizoguchi Y, Tsuchida K, Ichihashi T (2008) Enhancement of in vivo anticancer effects of cisplatin by incorporation inside single-wall carbon nanohorns. ACS Nano 2: 2057-2064.
60. Liu Z, Chen K, Davis C, Sherlock S, Cao Q (2008) Drug delivery with carbon nanotubes for in vivo cancer treatment. Cancer Res 68:6652-6660.
61. Chow EK, Zhang XQ, Chen M, Lam R, Robinson E (2011) Nanodiamond therapeutic delivery agents mediate enhanced chemo resistant tumour treatment. Sci Transl Med 3: 73-121.
62. Moore L, Chow EK, Osawa E, Bishop JM, Ho D (2013) Diamond-lipid hybrids enhance chemotherapeutic tolerance and mediate tumor regression. Adv Mater 25: 3532-3541.
63. Podesta JE, Al-Jamal KT, Herrero MA, Tian B, Ali-Boucetta H (2009) Antitumor activity and prolonged survival by carbon-nanotubemediated therapeutic siRNA silencing in a human lung xenograft model. Small 5: 1176-1185.
64. Soman NR, Baldwin SL, Hu G, Marsh JN, Lanza GM (2009) molecularly targeted nanocarriers deliver the cytolytic peptide melittin specifically to tumor cells in mice. Reducing tumor growth. J Clin Invest 119: 2830-2842.
65. Jensen SA, Day ES, Ko CH, Hurley LA, Luciano JP (2013) Spherical nucleic acid nanoparticle conjugates as an RNAi-

based therapy for glioblastoma. Sci Transl Med 5: 209-219.
66. Goldinger SM, Dummer R, Baumgaertner P, Mihic-Probst D, Schwarz K (2012) Speiser. Nano-particle vaccination combined with TLR -7 and -9 ligands triggers memory and effector CD8+ T-cell responses in melanoma patients. Eur J Immunol 42: 3049-3061.
67. Day ES, Zhang L, Thompson PA, Zawaski JA, Kaffes CC et al.,(2012) Vascular-targeted photothermal therapy of an orthotopic murine glioma model. Nanomedicine 7: 1133-1148.
68. Maggiorella L, Barouch G, Devaux C, Pottier A, Deutsch E et al., (2012) Nanoscale radiotherapy with hafnium oxide nanoparticles. Future Oncol 8: 1167-1181.
69. Kageyama S, Kitano S, Hirayama M, Nagata Y, Imai H et al., (2008) Humoral immune responses in patients vaccinated with 1–146 HER2 protein complexed with cholesteryl pullulan nanogel. Cancer Sci 99: 601-607.
70. Kitano S, Kageyama S, Nagata Y, Miyahara Y, Hiasa A et al, (2006) HER2-specific T-cell immune responses in patient's vaccinatedwith truncated HER2 protein complexed with nanogels of cholesteryl pullulan. Clin Cancer Res 12: 7397-7405.
71. Peoples GE, Holmes JP, Hueman MT, Mittendorf EA, Amin A et al., (2008) Combined clinical trial results of a HER2/neu (E75) vaccine for the prevention of recurrence in high-risk breast cancer patients: U.S. Military Cancer Institute Clinical Trials Group Study I-01 and I-02, Clin Cancer Res 14: 797-803.
72. Ali OA, Emerich D, Dranoff G, Mooney DJ (2009) In situ regulation of DC subsets and T cells mediates tumor regression in mice. Sci Transl Med 1: 8-19.
73. Pouponneau P, Leroux JC, Soulez G, Gaboury L, Martel S (2011) Co-encapsulation of magnetic nanoparticles and doxorubicin into biodegradable microcarriers for deep tissue targeting by vascular MRI navigation. Biomaterials 32: 3481-3486.
74. Garinot M, Fiévez V, Pourcelle V, Stoffelbach F, Rieux Ad et al., (2007) PEGylated PLGAbased nanoparticles targeting M cells for oral vaccination. J Control Release 120: 195-204.
75. Nguyen DN, Mahon KP, Chikh G, Kim P, Chung H et al., (2012) Lipid-derived nanoparticles for immunostimulatory RNA adjuvant delivery. Proc Natl Acad Sci U S A 109: 797-803.
76. Selbmann D, Bendjemil B, Leonhardt A, Pichler T, Täschner C et al., (2008) parametric study of the synthesis and purification of single-walled carbon nanotubes using the high-pressure carbon monoxide process. Applied Physics 90: 637-643.
77. Hayashi T, Hirono S, Tomita M, Umemura S (1996) Magnetic Thin Films of Cobalt Nanocrystals Encapsulated in Graphite-Like Carbon Nature 381: 722-774.
78. Costa S, Borowiak-Palen E, Bachmatiuk A, Rümmeli MH, Gemming T et al., (2007) Filling of carbon nanotubes for bio-applications 4315-4318.
79. Gökçen T, Dateo Ch E, Meyyappan M (2002) Modeling of the HiPco Process for Carbon Nanotube Production, II. Reactor-Scale Analysis. Journal of Nanoscience and Nanotechnology 2: 535-544.
80. Wang R, Zhang D , Zhang Y, Liu C (2006) Boron-doped carbon nanotubes serving as a novel chemical sensor for formaldehyde. J Phys Chem B 110: 18267-71.
81. Peng-Xiang H, Man S, Jin-Cheng L, Chang L, Shi-Sheng L et al., (2015) Synthesis of high quality nitrogen-doped single-wall carbon nanotubes.Science China Materials 58(8): 6603-610.
82. Mohammadi F Tavakol H (2018) Synthesis of phosphorus doped carbon nanotubes using chemical vapor deposition. Journal Fullerenes, Nanotubes and Carbon Nanostructures 26: 218-225.
83. Takeda N, Murakoshi (2007) Characteristics of the Raman spectra of single-walled carbon nanotube bundles under electrochemical potential control, Anal Bioanal Chem 388: 103-108.
84. Doorn SK, Heller DA, Barone PW, Usrey ML, Strano MS (2004) Resonant Raman excitation profiles of individually dispersed single walled carbon nanotubes in solution Appl Phys 78: 1147-1155.
85. Dresselhaus MS, Dresselhaus G, Jorio A, Souza AG, Pimenta MA et al., (2002) Single Nanotube Raman Spectroscopy, Acc Chem Res. 35: 1070-1078.
86. Dresselhaus MS, Dresselhaus G, Jorio A, Souza AG, Saito R (2002) Raman spectroscopy on isolated single wall carbon nanotubes Carbon 40: 2043-2016.
87. Dresselhaus MS, Dresselhaus G, Jorio A, Souza AG, Saito R (2002) Raman spectroscopy on one isolated carbon nanotube.